A Microdischarge-Based Deflecting-Cathode Pressure Sensor in a Ceramic Package

Scott A. Wright, *Member, IEEE*, Heidi Z. Harvey, and Yogesh B. Gianchandani, *Fellow, IEEE*

***Abstract*—This paper describes a microdischarge-based pressure sensor for harsh liquid environments that utilizes a ceramic package sealed with a deflecting diaphragm that also serves as a cathode. Located within the package is a reference cathode and an anode. The microdischarges are created between the two cathodes and the anode. The external pressure deflects the diaphragm, varying the interelectrode spacing and changing the differential current between the two competing cathodes. The electrodes are fabricated from a Ni foil and separated by dielectric spacers within a micromachined glass cavity. The structures are enclosed within a 1.6-mm^3 ceramic surface mount package. Device sensitivity is approximately 4900 ppm/lbf/in^2 (72 000 ppm/atm), and diaphragm displacement is approximately 0.15 μm/atm. [2011-0308]**

***Index Terms*—Plasma applications, plasma confinement, plasma measurements, plasma properties, pressure effects, sensitivity.**

I. Introduction

MICROSCALE pressure sensors that can withstand high pressures and temperatures are potentially useful for mining and subterranean exploration. A variety of optical and electrical approaches have been proposed for these and other various high-pressure and high-temperature applications. Some of the optical sensors that have been reported utilize interferometric structures, such as Fabry–Pérot cavities, which respond to applied pressure [1], [2]. The signal is carried by optical fibers. Other optical measurements use Bragg gratings, which are photoinscribed into optical fibers, to trace wavelength shifts caused by strain (or pressure and displacement) and temperature changes [3], [4]. The electrical approaches typically favor capacitive and piezoresistive transduction. Piezoresistive pressure sensors with diaphragms made from silicon carbide [5], and more recently even Si [6], have been reported that can also operate at elevated temperatures. Sapphire membranes have been also used in this context [7].

Microdischarges, or microplasmas, are miniature plasmas locally created in gases between electrodes. Microdischarges demonstrate characteristics different from those of plasmas created on a larger scale [8]; in general, microdischarges can be sustained at higher pressures, with much higher power densities and electric field strengths. Despite the high rate of collisions encountered at pressures approaching 1 atm, the electrons are in nonequilibrium, with much higher energy values than the ions [8]–[13]. When microdischarges are operating as glow discharges, ionization is based on the creation of high-energy secondary electrons. Microdischarge-based devices have been successfully demonstrated for applications in a variety of micro total analysis systems, including microscale optical emission spectroscopy systems for chemical sensing [14], [15].

A discharge-based approach to pressure sensing is complementary to conventional techniques. It offers simplicity in both electrical transduction and structural design, as well as the potential for wide dynamic range and temperature immunity. Devices utilizing microdischarges are well suited for high-temperature operation as the electrons have average thermal energy values exceeding 3 eV (34 815 K) [9] away from the cathode and small populations of very high-energy electrons with thermal energy values exceeding 400 eV near the cathode [10]. Ions have thermal energy values exceeding 0.03 eV above ambient (644 K) in a 23 °C (296 K) ambient environment. These energy levels allow the species to remain relatively immune to changes in ambient temperature. For example, a microdischarge-based vacuum level sensor that exploits the variation, with pressure, of the mean free path of gas molecules was previously reported [16]. It used an unsealed structure fabricated and operated in clean gas environments up to 2.5 atm and 1000 °C. This type of sensor is different from an ion gauge; an ion gauge cannot be designed to operate at atmospheric pressure because the small mean free path of the ions, i.e., 20–65 nm, makes these difficult to detect at the collector [17].

This paper describes a microdischarge-based pressure sensor for harsh liquid environments that utilizes a ceramic package sealed with a deflecting diaphragm that also serves as a cathode. Located within the package is a second (stationary reference) cathode and an anode.[1] It operates by measuring the deflection of the diaphragm electrode resulting from external pressure. An increase in applied pressure deflects the diaphragm toward the anode, altering the current distribution between the two cathodes. This creates a differential current readout, which is used for measurement. Instead of a multicathode arrangement, multiple anodes may be used; however, anode current shows very high dependence on encapsulated gas pressure [10]. This high sensitivity results in relatively small dynamic ranges,

Manuscript received October 20, 2011; revised August 5, 2012; accepted August 17, 2012. This work was supported by the Advanced Energy Consortium. Subject Editor H. Fujita.

S. A. Wright is with Exponent Failure Analysis Associates, Inc., Menlo Park, CA 94025 USA (e-mail: scottwri@umich.edu).

H. Z. Harvey is with Sandia National Laboratories, Albuquerque, NM 87185 USA.

Y. B. Gianchandani is with the Department of Electrical Engineering and Computer Science, University of Michigan, Ann Arbor, MI 48109 USA.

Color versions of one or more of the figures in this paper are available online at http://ieeexplore.ieee.org.

Digital Object Identifier 10.1109/JMEMS.2012.2215009

[1]Portions of this paper have been reported in conference abstract form [18].

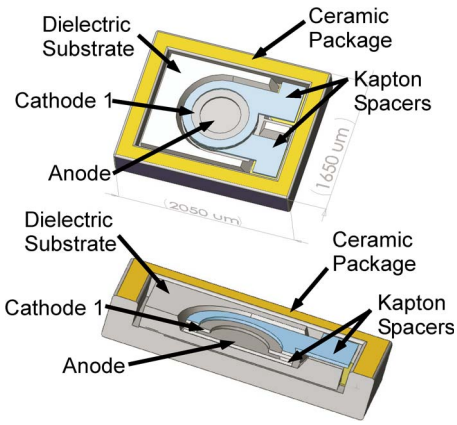

Fig. 1. Schematic of device contained within a commercial Kyocera package.

thereby limiting the utility of multianode configurations. The electrodes are made from bulk metal foil and arranged in a stack within a quartz substrate. The active volume of these devices is 0.057 mm^3, which is $\approx 10\times$ smaller than previously reported microdischarge-based pressure sensors with active volumes of 0.412 mm^3 [16]. The pressure range is $\approx 6\times$ higher. The design of the device and microdischarge operation are described in Section II, whereas fabrication processes are addressed in Section III. The sensors are tested in an oil environment with a desired operating range from 1–15 atm. Experimental results are provided in Section IV.

II. Device Design and Operation

The pressure sensors consist of a microdischarge chamber formed within a commercial package (see Fig. 1). A single disk-shaped anode electrode serves as the bottom of the chamber. The center electrode (cathode 1) is torus shaped, allowing the discharges to exist between the bottom anode and both cathodes. The package sealing diaphragm electrode (cathode 2) serves as the top of the chamber. Epoxy can be also used as an insulating layer above this cathode. Each electrode is connected to a package feedthrough lead. The electrodes are made of thin foil nickel. Nickel offers several benefits.

1) It produces a single uniform discharge for each applied current pulse, as opposed to numerous sporadic discharges produced by electrodes made from cold-rolled steel and other materials.
2) It has a high secondary electron emission coefficient (i.e., 0.034 secondary electrons created per incident 10-eV Ar^+ ion [19]), which further facilitates microdischarges.
3) It is more resistant to oxidation than alternatives such as stainless steel and copper.

Dielectric spacers made from Kapton are used between electrodes to maintain interelectrode spacing and provide electrical isolation. These spacers are torus shaped to maintain and define the through hole between the fixed anode and two cathodes. A dielectric Pyrex substrate is used within the package to maintain the position of the electrodes in their stacked structure and isolate them from the ceramic package. The microdischarge chamber exists in the center of the package, in the through hole created by the electrodes and spacers.

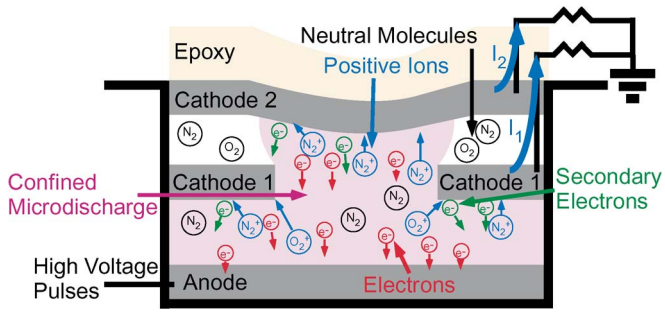

Fig. 2. Diagram of a microdischarge between a single anode and two cathodes.

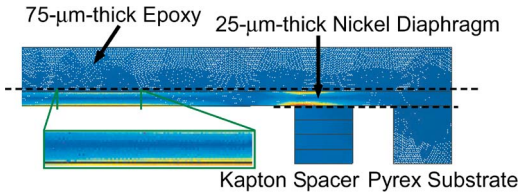

Fig. 3. Stress analysis indicating regions of elevated stress, at 100 lbf/in^2 (690 kPa), of a 25-μm-thick nickel diaphragm with 75-μm-thick epoxy encapsulation performed using COMSOL.

The encapsulated microdischarge-based sensors operate by measuring changes in current distribution of pulsed dc microdischarges between the anode and two cathodes. The distal diaphragm cathode 2 deflects due to external pressure, changing the interelectrode spacing, as shown in Fig. 2. To determine the pressure causing this deflection, it is first necessary to separately determine the current in the two cathodes. These current components are denoted as I_1 in cathode 1 and I_2 in cathode 2. The differential current, expressed as a fraction of the total peak current $(I_1 - I_2)/(I_1 + I_2)$, is treated as the sensor output. At lower pressures, cathode 2 is deflected less and more current flows through cathode 1, whereas at higher pressures, more current flows through cathode 2. An important benefit of using a differential output that is expressed as a fraction of the total is that the exact magnitudes are less important than fractional changes. This distinction also minimizes variation in sensor output due to anomalies in the manufacturing and assembly of the components and the interelectrode spacing.

A. Diaphragm Analysis

The nature of the deflecting diaphragms has a significant impact on the operating parameters of the pressure sensors. Thinner diaphragms have a lower operating pressure range but provide higher sensitivity, whereas thicker diaphragms could operate over a large pressure range at limited sensitivity. The solid model used for finite-element analysis (FEA) includes the electrode–spacer stack and the Pyrex substrate, although the ceramic package is not included. Hence, the compression of the Kapton spacers is taken into consideration. The FEA results of a 25-μm-thick nickel diaphragm encapsulated with approximately 75-μm-thick epoxy that serves as an insulating seal are shown in Fig. 3; the experimental measurements are taken using this type of diaphragm. The regions of maximum stress are at the interface between the diaphragm and a Kapton

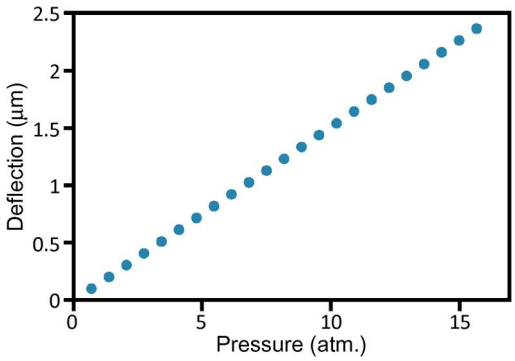

Fig. 4. Simulated deflection at the center of the diaphragm, as a function of external pressure.

spacer, and in the center of the diaphragm where the deflection is largest. The deflection in the diaphragm center is about 0.15 μm/atm; the deflection is plotted as a function of pressure in Fig. 4.

B. Internal Pressure Increase Due to Diaphragm Deflection

A secondary influence on the microdischarge current is caused by the change in pressure within the sealed cavity that results from the diaphragm displacement. As the diaphragm deflects, the chamber internal pressure slightly increases and the mean free path of the gas in the microdischarge is likewise shortened. This change in mean free path alters the current distribution to the two cathodes, with current favoring the distal cathode at lower internal pressures and favoring the proximal cathode at higher internal pressures. This change in current distribution is the opposite of that due to diaphragm deflection and diminishes the overall sensitivity.

The deflection at the center of a circular diaphragm is given by [20]

$$\Delta d = \frac{3 \cdot \Delta P (1 - v^2) a^4}{16 E h^3} \tag{1}$$

where ΔP is the pressure difference across the diaphragm, a is the radius, h is the thickness, v is Poisson's ratio of the material, and E is Young's modulus. This is valid for a thin diaphragm with simply supported edges, assuming a small deflection. The volume change resulting from a pressure difference is [20]

$$\Delta V = \frac{3\pi \cdot \Delta P \left(1 - v^2\right) a^6}{48 E h^3}. \tag{2}$$

Using (1) and (2), the volume change is related to the central deflection and the diaphragm area by

$$\Delta V = \frac{\pi \cdot a^2 \cdot \Delta d}{3}. \tag{3}$$

Using a linear fit to the plot in Fig. 4, the center of the diaphragm deflects approximately 150 nm/atm. The radius of the deflecting diaphragm, as defined by contact with the Kapton spacer, is 325 μm, and the volume of air sealed at 1 atm within the cavity is 0.146 mm^3. The volume changes by 16 591 μm^3/atm or 0.011%. By the ideal gas law, the percentage change in volume of the air encapsulated is inversely proportional to its change in pressure; hence, the anticipated change in pressure in the interior cavity is 0.0836 torr/atm. With an external pressure of 15 atm, the maximum internal pressure is 761.3 torr. We have previously shown that at pressures up to about 2 atm, microdischarges of similarly spaced electrodes have a maximum sensitivity of 5420 ppm/torr or 7.1 ppm/atm to the discharge cavity pressure [16]. This suggests that the sealed sensors described here would have a sensitivity of -0.78 ppb/atm if the deflection did not directly affect the microdischarge. As shown below in the experimental measurements, this sensitivity is orders of magnitude smaller than the measured sensitivity, and hence, it is evident that this mechanism does not meaningfully contribute to the response.

C. Microdischarge Operation and Theoretical Considerations

Fig. 2 illustrates the electron and ion transport that allows dc microdischarge operation within the diaphragm-sealed cavity. The electrons are drawn toward the anode, whereas the positive ions are drawn to the two separate cathodes forming positively charged sheaths around them. Upon cathode impact, the energetic ions eject high-energy secondary electrons from the cathodes, which sustain the microdischarge by ionizing additional neutral molecules and continuing the breakdown process. High-energy ions are encountered in microdischarge as a result of the high power densities and voltage gradients encountered in the small gap spacing. The current in each cathode is composed of a combination of positive ions impacting the cathodes from the microdischarge and secondary electrons ejected from the cathodes upon ion impact. Further away from the cathodes, the current is carried primarily by the faster moving electrons, which cannot reach the cathodes because of the surrounding sheaths.

Sensor characteristics such as sensitivity, pressure dynamic range, and temperature dynamic range depend on a variety of dimensional parameters, including interelectrode spacing, electrode diameter, and cathode thickness. (Cathode thickness affects sheath sizes and electrode positioning.) In this effort, the sensors are designed to function with an applied voltage of 500 V; altering the voltage results in different sensitivities.

Power consumption and parasitic heating in the pressure sensors are controlled by using pulsed dc microdischarges, as opposed to constant dc discharges. The use of pulsed powering creates high-current pulse arcs, which initiate the microdischarges as described by several authors [21]–[23]. The magnitudes of the current pulses show much greater sensitivity to pressure than the sustained dc current levels.

The microdischarge current pulses measured at each of the two cathodes can be modeled by an equivalent circuit (see Fig. 5). The pulse power source is represented by discharging of a capacitor C, whereas the current pulse is shaped by a series combination of an inductance L and resistance R, as developed by Robiscoe *et al.* [24], [25]. A shunt resistance R_s permits a leakage current I_s to drain the capacitor, even in the absence of a discharge. As all of the circuit elements are passive, the relationships between voltage drops across the circuit elements can be described by a linear system of differential equations with constant coefficients. The equations

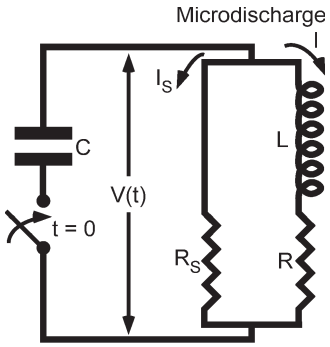

Fig. 5. Equivalent circuit model for microdischarge currents. The pulse power source is represented by discharging of the capacitor C that is switched on at time $t = 0$. The current pulse is shaped by an equivalent circuit represented by two resistors and an inductor.

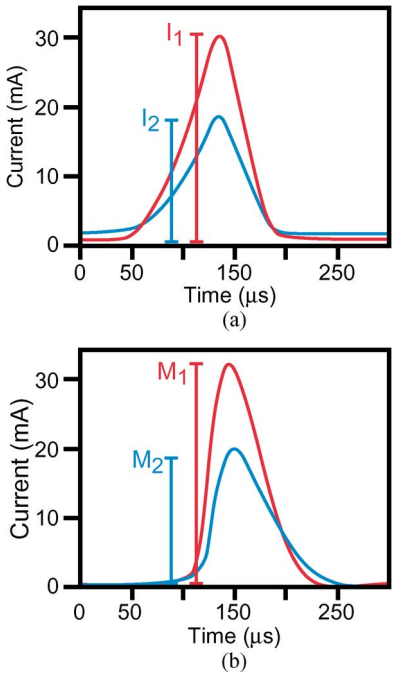

Fig. 6. (a) Experimentally measured and (b) fitted current pulses in cathodes 1 and 2 in a pressure sensor with electrodes spaced 25 μm apart, 800 μm in diameter, and 25-μm thick at 100 lbf/in^2.

relating microdischarge peak current, pulse duration, and pulse rise time to circuit elements are described specifically in [16].

Microdischarge pulses are experimentally measured for a pressure sensor with electrodes 800 μm in diameter, spaced nominally 25 μm apart, and 25-μm thick at a pressure of 690 kPa (100 lbf/in^2) and with a pulsed voltage of 500 V. The pulses in both cathodes are shown in Fig. 6(a), displaying overdamped current oscillations without ringing or secondary pulses. For cathode 1, the peak current is 31 mA; the pulse duration, measured from initiation to the I_p/e time, is 165 μs; and the pulse rise time is 80 μs. For cathode 2, the parameters are 19 mA, 140 μs, and 50 μs, respectively. The circuit element values were determined by fitting the modeled microdischarge pulses to the experimentally obtained pulses. The microdischarge through cathode 1 is modeled with a R of 300 Ω, a C of 3.3 nF, and an L of 180 mH. The microdischarge through cathode 2 is modeled with a R of 300 Ω, a C of 2.6 nF, and an L of 250 mH. R_S is 5.5 kΩ. Fig. 6(b) shows the modeled current pulses in the pressure sensor described above as plotted in SPICE. Similar analysis can be applied to determine the circuit elements for other pressure sensor configurations. However, it is evident from Fig. 6 that the equivalent circuit models provide only approximate representations of the microdischarge currents. (First-principle Monte Carlo models for pulsed microdischarges are being developed, but they are beyond the scope of this effort.)

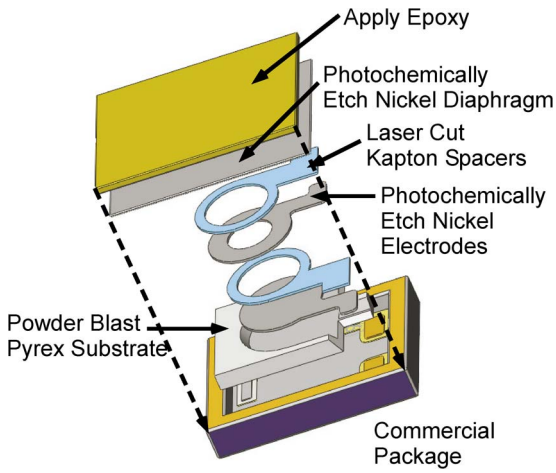

Fig. 7. Component integration illustrating a stacked electrode/spacer structure within a commercial package before diaphragm attachment.

III. Fabrication

The sensor elements are assembled into commercial packages. A dielectric substrate is inserted into the package, and the bulk metal electrodes and dielectric spacers are stacked within it. All of these components are sealed within by bonding a metal diaphragm to the package opening, as shown in Fig. 7.

The package used in this effort is a ceramic package designed for crystal oscillators and has external dimensions of $2.05 \times 1.65 \times 0.5$ mm^3 (Kyocera, Japan). The package has two internal feedthroughs with gold-coated contact pads, which are used for connection to the anode and cathode 1. A third gold-coated contact pad on the rim makes electrical contact to cathode 2, i.e., the diaphragm. It also serves at the bonding ring when the lid is solder sealed.

The substrate is composed of 175-μm-thick Pyrex. It maintains the position of the electrodes and dielectric spacers within the package. It also provides electrical isolation of the electrodes and package limiting electrical connection to the two feedthroughs. The sidewalls of the substrate and the recessed area in the center are formed using a microabrasive-jet (MAJ) process, also known as powder abrasive blasting (Bullen Ultrasonics, Eaton, OH). The substrates are formed from Schott D263 borosilicate glass due to its machinability and dielectric properties. The MAJ process is used because it allows a 100-μm-deep recess to be etched into the center of the substrates while maintaining a high-aspect-ratio sidewall. The microdischarge chambers exist within this recess.

The electrodes are lithographically patterned and etched from foil using photochemical machining [26]. This process

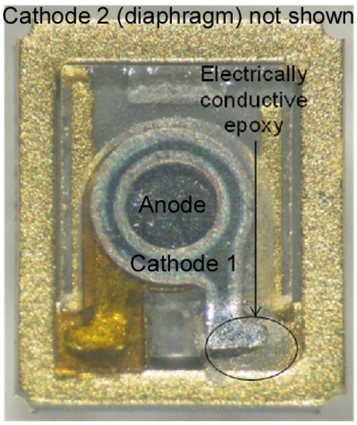

Fig. 8. Assembled device illustrating the composition of all components, excluding deflecting diaphragm lid, and exhibiting conductive epoxy used to hold the anode and cathode 1 in place. Kapton layers have a yellow color and insulate the electrodes.

involves coating a thin sheet of metal with photoresist, exposing the resist, and spraying the sheet with a chemical etchant to dissolve the exposed metal. The exposed metal is completely removed, leaving through holes in the sheet, and the resist is stripped (ChemArt Company, Lincoln, RI). For this effort, the electrodes are made 25-μm thick with outer diameters of 800 μm. The inner diameter of cathode 1, i.e., the torus-shaped electrode, is 480 μm. This inner diameter defines the area of the center through hole in which discharges occur. The electrodes are patterned from nickel, which is robust, inexpensive, easily machinable by microelectrodischarge machining and photochemical etching, and has a sufficiently high secondary emission coefficient in an air ambient. While its yield strength is lower than that of other options such as stainless steel, thus limiting the maximum pressure, its microdischarge characteristics are superior. (Cold-rolled steel diaphragms require a nickel coating to provide the necessary discharge characteristics.)

The dielectric torus-shaped spacers serve to electrically isolate the electrodes from one another and from the diaphragm and to allow microdischarges to be created in their center through holes. They also define the interelectrode spacing. The spacers are laser cut from a Kapton sheet (Tech-Etch, Plymouth, MA). For this effort, the spacers are 25-μm thick. Some compression of the Kapton occurs when pressure is applied. However, due to the nature of the sensor output, a fractional change rather than an analysis of precise values, this compression does not affect sensor operation. Kapton is used because of its dielectric properties and ability to withstand temperatures up to 400 °C without significant dielectric loss.

In the earlier version of the sensors, the electrodes are connected to the electrical pads of the package and feedthroughs by conductive silver epoxy (see Fig. 8). The epoxy also physically secures the electrodes. The diaphragm is bonded to the package using a laser welding or solder bonding technique. During laser welding, a 200-μm-diameter laser is used to locally heat the side of the package and the diaphragm. This technique does not require any preliminary metal deposition and can be used with any diaphragm thickness. It works for nickel and other metals as well. When solder bonding, a micromachined Sn/Pb foil bond ring is used between the package and the diaphragm.

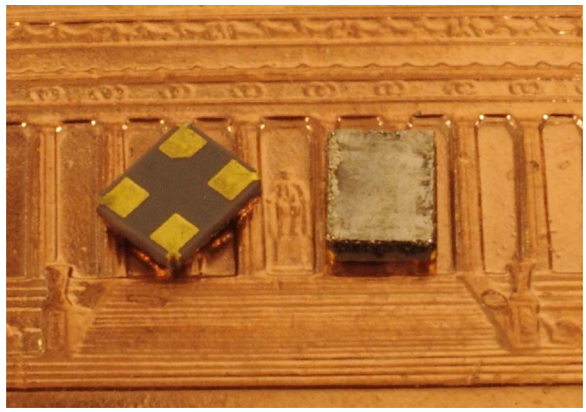

Fig. 9. Photograph of pressure sensors with laser-welded diaphragms on a penny.

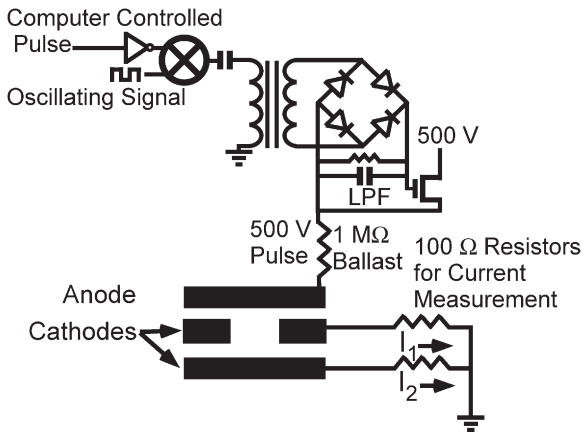

Fig. 10. Schematic of the computer-controlled, single-ended, transformer-coupled, gate drive circuit used to create pulses.

The package is placed in a header that allows pressure to be applied on the lid while it is being heated. With applied heat and pressure, the solder foil melts and bonds the lid to the package. This method does add some space between the final spacer and the diaphragm lid; however, due to the nature of the sensor output, this added thickness does not significantly affect sensor operation. These bonding procedures hermetically seal the components within the package. The diaphragm rests on the electrode/spacer stack to strictly define the maximum interelectrode spacing between it and cathode 1. Both methods seal the package with gas (in this case, air) encapsulated within it. Sensors with laser-welded diaphragms are shown in Fig. 9.

IV. Results

Pressure sensors were fabricated and tested at pressures up to 15 atm (220 $\mathrm{lbf/in^2}$) in dielectric oil. To control power consumption and parasitic heating in the pressure sensors, pulsed dc microdischarges were used as opposed to constant dc discharges. A computer-controlled, single-ended, transformer-coupled, gate drive circuit created the pulses. Pulses 1 ms in duration and with an amplitude of 500 V were applied. This amplitude was sufficient to cause gas breakdown during every pulse. A current-limiting 1-MΩ ballast resistor was used in series with the anode; moreover, 100-Ω resistors were used in series with each cathode to measure I_1 and I_2 (see Fig. 10).

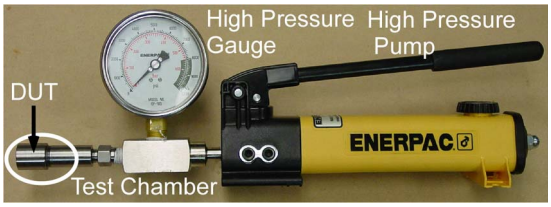

Fig. 11. Test setup used to apply high-pressure oil to the sensors.

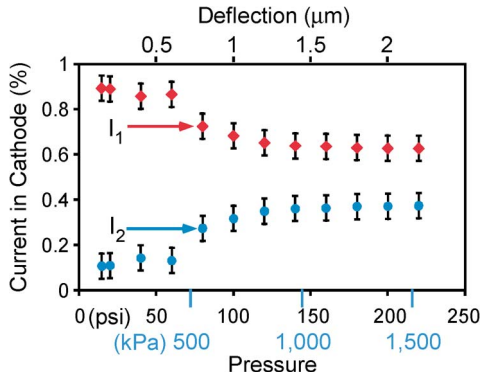

Fig. 12. Current distribution between cathodes 1 and 2 in a sensor with a 25-μm-thick nickel diaphragm encapsulated with a 75-μm-thick epoxy layer. Each data point is the average of 100 measurements.

The applied voltage pulses resulted in current pulses through each cathode. The transient current peaks were approximately 100–200 μs in duration, with amplitudes of 5–50 mA (250 μJ per pulse), varying with pressure. Pressure was determined by measuring the difference between the fractional current in each cathode. Experimentally obtained pulses in both cathodes are shown in Fig. 6(a), displaying overdamped current oscillations.

To create the high-pressure environments, compressed nitrogen was used to pressurize the oil at lower pressures while a hydraulic jack shown in Fig. 11 was used at higher pressures. Devices were attached to a custom pressure header, which allowed electrical connection within this test structure.

A sensor fabricated with a 25-μm-thick nickel diaphragm was coated with an approximately 75-μm-thick epoxy layer that served as an insulating seal. The sensor was attached to the custom pressure header and subjected to high-pressure oil applied by the hydraulic jack. The fractional current distribution between cathodes 1 and 2 produced by the sensor as a function of pressure is shown in Fig. 12. This fractional distribution is as expected at low pressures: When the diaphragm is not significantly deflected, the current favors the cathode proximal to the anode, i.e., cathode 1; at higher pressures, when the diaphragm is deflected to a larger extent, the current favors the deflected distal cathode 2 to a greater extent. The final differential sensor output is shown in Fig. 13. Each data point is the average of 100 consecutive measurements, although the data at 60 $\mathrm{lbf/in^2}$ slightly deviated from the trend. This particular sensor was able to measure pressure up to 15 atm and provided a sensitivity of 4900 $\mathrm{ppm/lbf/in^2}$ (72 000 ppm/atm) averaged over the operating pressure range of the device.

V. Conclusion

Encapsulated microdischarge-based pressure sensors have demonstrated an ability to measure pressure up to 15 atm

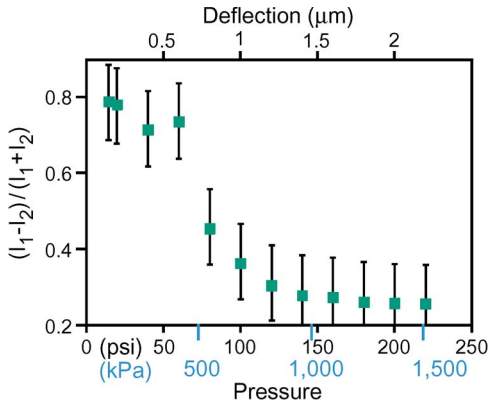

Fig. 13. Sensor output as a function of pressure in a sensor with a 25-μm-thick nickel diaphragm encapsulated with a 75-μm-thick epoxy layer.

within oil environments. These sensors have demonstrated microdischarge-based proximity sensing in this work of a pressure-deflected diaphragm. By utilizing different diaphragm materials and thicker diaphragms, the dynamic range of the sensors can be expanded, possibly even to pressures as high as 20 000 $\mathrm{lbf/in^2}$ as experienced in petroleum exploration and pumping. The electrical nature of the readout avoids an intermediate transduction step that is common to many sensors. The discharge-based transduction also provides a large readout that does not require local amplification, although it does require a high-voltage (pulsed) power source. These two factors provide a simplicity that is very attractive to systems that may involve many embedded sensors or utilize portable applications.

Acknowledgment

The authors would like to thank Dr. J. Shah of Schlumberger Corporation for guidance on testing methods and Dr. C. Eun of the University of Michigan, Ann Arbor, for the assistance with the finite-element analysis.

References

[1] R. S. Fielder, K. Stingson-Bagby, and M. Palmer, "State of the art in high-temperature fiber optic sensors," *Proc. SPIE*, vol. 5589, pp. 60–413, Dec. 2004.

[2] D. C. Abeysinghe, S. Dasgupta, H. E. Jackson, and J. T. Boyd, "Novel MEMS pressure and temperature sensors fabricated on optical fibers," *J. Micromech. Microeng.*, vol. 12, no. 3, pp. 229–235, Mar. 2002.

[3] T. Li, Z. Wang, Q. Wang, X. Wei, B. Xu, W. Hao, F. Meng, and S. Dong, "High pressure and temperature sensing for the downhole applications," in *Proc. SPIE*, Oct. 2007, pp. 675706-1–675706-7.

[4] Y. Zhao, Y. Liao, and S. Lai, "Simultaneous measurement of downhole high pressure and temperature with a bulk-modulus and FBG sensor," *IEEE Photon. Technol. Lett.*, vol. 14, no. 11, pp. 1584–1586, Nov. 2002.

[5] A. Ned, R. Okojie, and A. Kurtz, "6H-SiC pressure sensor operation at 600 °C," in *Proc. Int. High Temp. Electron. Conf.*, Albuquerque, NM, 1998, pp. 257–260.

[6] S. Guo, H. Eriksen, K. Childress, A. Fink, and M. Hoffman, "High temperature high accuracy piezoresistive pressure sensor based on smart-cut SOI," in *Proc. IEEE Int. Conf. Micro Electro Mech. Syst.*, Tucson, AZ, 2008, pp. 892–895.

[7] S. Fricke, A. Friedberg, T. Ziemann, E. Rose, G. Muller, D. Telitschkin, S. Ziegenhagen, H. Seidel, and U. Schmidt, "High temperature (800 °C) MEMS pressure sensor development including reusable packaging for rocket engine applications," in *Proc. Micro-Nano-Technol. Aerosp. Appl. CANEUS*, Toulouse, France, 2006, pp. 287–291.

[8] R. Foest, M. Schmidt, and K. Becker, "Microplasmas, an emerging field of low-temperature plasma science and technology," *Int. J. Mass Spectrom.*, vol. 248, no. 3, pp. 87–102, Feb. 2006.
[9] M. Kushner, "Modeling of microdischarge devices: Plasma and gas dynamics," *J. Phys. D, Appl. Phys.*, vol. 38, no. 11, pp. 1633–1643, Jun. 2005.
[10] C. G. Wilson, Y. B. Gianchandani, R. Arslanbekov, V. Kolobov, and A. Wendt, "Profiling and modeling of dc nitrogen microplasmas," *J. Appl. Phys.*, vol. 94, no. 5, pp. 2845–2851, Sep. 2003.
[11] J. G. Eden and S.-J. Park, "Microcavity plasma devices and arrays: A new realm of plasma physics and photonic applications," *Plasma Phys. Control. Fusion*, vol. 47, no. 12B, pp. B83–B92, Nov. 2005.
[12] J. Choi, F. Iza, J. K. Lee, and C. Ryu, "Electron and ion kinetics in a dc microplasma at atmospheric pressure," *IEEE Trans. Plasma Sci.*, vol. 35, no. 5, pp. 1274–1278, Oct. 2007.
[13] Y. J. Hong, S. M. Lee, G. C. Kim, and J. K. Lee, "Modeling high-pressure microplasmas: Comparison of fluid modeling and particle-in-cell Monte Carlo collision modeling," *Plasma Process. Polym.*, vol. 5, no. 6, pp. 583–592, 2008.
[14] V. Karanassios, "Microplasmas for chemical analysis: Analytical tools or research toys?" *Spectrochim. Acta B, At. Spectrosc.*, vol. 59, no.7, pp. 909–928, Jul. 2004.
[15] B. Mitra and Y. B. Gianchandani, "The detection of chemical vapors in air using optical emission spectroscopy of pulsed microdischarges from two and three electrode microstructures," *IEEE Sensors J.*, vol. 8, no. 8, pp. 1445–1454, Aug. 2008.
[16] S. A. Wright and Y. B. Gianchandani, "Discharge-based pressure sensors for high-temperature applications using three-dimensional and planar microstructures," *J. Microelectromech. Syst.*, vol. 18, no. 3, pp. 736–743, Jun. 2009.
[17] C. Edelmann, "Measurement of high pressures in the vacuum range with the help of hot filament ionization gauges," *Vacuum*, vol. 41, no. 7–9, pp. 2006–2008, 1990.
[18] S. A. Wright, H. A. Zipperian, and Y. Gianchandani, "A 15 atm. pressure sensor utilizing microdischarges in a 1.6 mm^3 ceramic package," in *Proc. Solid-State Sens. Actuators Microsyst. Workshop*, Hilton Head, SC, 2010, pp. 53–56.
[19] Y. Takeishi and H. D. Hagstrum, "Auger-type ejection from the (111) face of nickel by slow He^+, Ne^+, and Ar^+ ions," *Phys. Rev.*, vol. 137, no. 2A, pp. A641–A647, Jan. 1965.
[20] M. Gad-el-Hak, Ed., *The MEMS Handbook*, 2nd ed. Boca Raton, FL: CRC Press, 2006.
[21] D. Staack, B. Farouk, A. Gutsol, and A. Fridman, "Characterization of a dc atmospheric pressure normal glow discharge," *Plasma Sources Sci. Technol.*, vol. 14, no. 4, pp. 700–711, Nov. 2005.
[22] H. Rahanman, B. Lee, I. Petzenhauser, and K. Frank, "Switching characteristics of microplasmas in a planar electrode gap," *Appl. Phys. Lett.*, vol. 90, no. 13, pp. 131505-1–131505-3, Mar. 2007.
[23] J. Choi, K. Matsuo, H. Yoshida, T. Namihira, S. Katsuki, and H. Akiyama, "Characterization of a dc-driven atmospheric pressure air microplasma jet," *Jpn. J. Appl. Phys.*, vol. 47, no. 8, pp. 6459–6463, Aug. 2008.
[24] R. T. Robiscoe and Z. Sui, "Circuit model of surface arcing," *J. Appl. Phys.*, vol. 64, no. 9, pp. 4364–4374, Nov. 1988.
[25] R. T. Robiscoe, A. Kadish, and W. B. Maier, II, "A lumped circuit model for transient arc discharges," *J. Appl. Phys.*, vol. 64, no. 9, pp. 4355–4363, Nov. 1988.
[26] D. M. Allen, "The state of the art of photochemical machining at the start of the twenty-first century," *Proc. Inst. Mech. Eng. B, J. Eng. Manuf.*, vol. 217, no. 5, pp. 643–650, 2003.

Scott A. Wright (M'09) received the B.S. degree in electrical engineering from the University of California, Los Angeles, in 2004, and the M.S. and Ph.D. degrees in electrical engineering from the University of Michigan, Ann Arbor, in 2006 and 2009, respectively, with a focus on circuits and microsystems.

He is currently with the Electrical Engineering and Computer Science Practice, Exponent Failure Analysis Associates, Inc., Menlo Park, CA, where he focuses on circuit failure analysis, fire investigation, prototype characterization, microscale devices, plasma science, and spectroscopy. He has previously worked with Lockheed Martin Corporation, Sunnyvale, CA, and Bell Laboratories, Florham Park, NJ. His research interests include the study of plasma physics at the micrometer scale; microdischarges; and applications of microdischarges in micropumps, pressure sensors, and spectroscopic sensors.

Dr. Wright received the Armed Forces Communications and Electronics Association Fellowship for his work with microplasmas. He was the University of Michigan MIT Lincoln Laboratory Graduate Fellow for 2007–2008.

Heidi Z. Harvey (M'08) received the B.S. degree in general engineering with a concentration in electrical engineering from Arizona State University, Tempe, in 2009, and the M.S. degree in electrical engineering from the University of Michigan, Ann Arbor, in 2011, with a focus in circuits and microsystems. She is currently studying biomedical engineering at the University of New Mexico, Albuquerque.

She is also currently with Sandia National Laboratories, Albuquerque, NM, working in MEMS technologies. Her research interests include MEMS and their applications to medical technology, specifically drug delivery.

Yogesh B. Gianchandani (S'86–M'86–SM'05–F'10) received the B.S. degree from the University of California, Irvine, in 1984, the M.S. degree from the University of California, Los Angeles, in 1986, and the Ph.D. degree from the University of Michigan, Ann Arbor, in 1994, all in electrical engineering.

He is currently a Professor at the University of Michigan, Ann Arbor, with a primary appointment in the Department of Electrical Engineering and Computer Science and a courtesy appointment in the Department of Mechanical Engineering. He also serves as the Director of the Center for Wireless Integrated MicroSensing and Systems ($WIMS^2$). His research interests include all aspects of design, fabrication, and packaging of micromachined sensors and actuators and their interface circuits. He has published more than 250 papers in journals and conference proceedings and has about 35 U.S. patents issued or pending. He was a Chief Coeditor of Comprehensive Microsystems: Fundamentals, Technology, and Applications, published in 2008.

Dr. Gianchandani serves several journals as an Editor or a Member of the Editorial Board. He served as General Cochair for the IEEE/ASME International Conference on Micro Electro Mechanical Systems (MEMS) in 2002. From 2007 to 2009, he also served at the National Science Foundation as the Program Director for Micro and Nano Systems within the Electrical, Communication, and Cyber Systems Division (ECCS).